Geochemical Perspectives Letters

Fe-H melting curve below 3 GPa: implications for hydrogen in the lunar core

J. Takeshita[1], K. Hirose[1,2*], S. Fu[3], F. Sakai[1], K. Hikosaka[1,4]

OPEN ACCESS

https://doi.org/10.7185/geochemlet.2633

Abstract

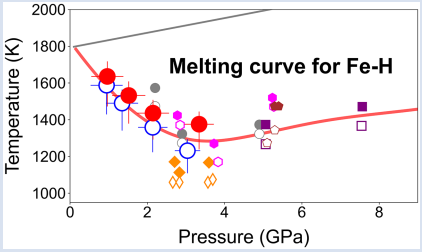

It has been assumed that hydrogen is negligibly incorporated into core forming metals below ~3 GPa, and therefore the presence of hydrogen in iron cores of small terrestrial bodies including the moon has not been considered. Here we performed high pressure melting experiments on the Fe-H system under H_2 saturated conditions, combined with synchrotron X-ray diffraction (XRD) measurements. Results demonstrate substantial depression of the Fe-H melting curve compared to that for Fe at 1.0–3.3 GPa, indicating that hydrogen is incorporated into liquid iron even at low pressures (less than 1 GPa) and the solubility is enhanced with increasing pressure. Based on the density of liquid Fe-H derived from diffuse scattering signal in XRD data, we found that the solubility of hydrogen in liquid iron is about 0.9 wt. % at 3.6 GPa and likely enhanced to 1.1 wt. % at 5 GPa corresponding to lunar core conditions. The 1.1 wt. % H causes 9 % density reduction, which might fully explain the observed density deficit of the lunar core with respect to iron, depending on the density estimate from seismological data, although the presence of sulfur and carbon is not excluded.

Received 24 February 2026 | Accepted 7 August 2026 | Published 15 September 2026

Introduction

Geophysical constraints on the lunar interior indicate that the density of its core is a few percent up to ~40 % lower than that of pure iron (*e.g.*, Garcia *et al.*, 2019; Viswanathan *et al.*, 2019; Kuskov *et al.*, 2021; Zhao *et al.*, 2023). Such density deficit requires the presence of substantial amounts of light elements in the metallic core, and sulfur and carbon have often been regarded as possible light alloy elements (*e.g.*, Jing *et al.*, 2014; Steenstra *et al.*, 2017). In contrast, hydrogen has received comparatively less attention since stoichiometric FeH is formed from Fe and H_2 only above 3.5 GPa at room temperature (Badding *et al.*, 1991). Indeed, hydrogen was assumed to be poorly soluble into iron below ~3 GPa in recent core formation modelling (Tagawa *et al.*, 2021; Tsutsumi *et al.*, 2025).

Only a limited number of high pressure and temperature (*P-T*) experiments were previously reported on the Fe-H system below 3 GPa. All neutron diffraction measurements on Fe-H alloys have been carried out at pressures of ~3 GPa, and at temperatures far below the onset of melting (*e.g.*, Iizuka-Oku *et al.*, 2017; Machida *et al.*, 2019; Ikuta *et al.*, 2019). Yagi and Hishinuma (1995) performed XRD measurements on Fe-H and determined melting temperatures at pressures down to 2.2 GPa, demonstrating a large reduction from the melting curve of Fe. Other experimental studies reported the Fe(-Ni)-H melting temperatures only above 2.7 GPa (Suzuki *et al.*, 1984; Okuchi, 1998; Fukai *et al.*, 2003; Sakamaki *et al.*, 2009; Shibazaki *et al.*, 2014; Mita *et al.*, 2025).

In this study, we focus on Fe-H melting experiments below ~3 GPa to explore the enhancement of hydrogen solubility in iron with increasing pressure. The results show the clear melting temperature depression even at 1.0 GPa and higher hydrogen concentrations in liquid and solid iron at higher pressures, suggesting that hydrogen could be an important light element in metallic iron cores of small terrestrial bodies. We discuss the possible hydrogen abundance in the lunar core based on seismological constraints on its density.

Results

We conducted melting experiments on the Fe + H_2 sample at four different *P-T* conditions (laser heating was performed at two separate portions of a sample in each of two independent runs) (Table S-1). In run #1, after compression under 300 K to 1.1 GPa, we first heated the sample at spot #1-1 and observed a diffuse scattering signal indicative of melting, along with the XRD peaks from face centred cubic (fcc) $FeH_{0.16}$, when temperature was increased from 1490 K at 1.3 GPa to 1530 K at 1.5 GPa (Fig. 1). After quenching to 300 K, we decompressed the sample to 0.6 GPa and then heated a fresh sample portion (spot #1-2) being exposed to X-ray and laser beams. XRD data exhibited a diffuse scattering signal from liquid upon increasing temperature from 1590 K to 1710 K at 1.0 GPa. While the diffuse signal persisted, coexisting with fcc $FeH_{0.08}$ upon decrease in temperature to 1640 K, it disappeared when we decreased the sample

1. Department of Earth and Planetary Science, The University of Tokyo, Tokyo 113-0033, Japan
2. Earth-Life Science Institute, Institute of Science Tokyo, Tokyo 150-8550, Japan
3. School of Earth Sciences, Zhejiang University, Hangzhou 310058, China
4. Department of Earth and Planetary Sciences, Institute of Science Tokyo, Tokyo 150-8551, Japan
* Corresponding author (email: kei@eps.s.u-tokyo.ac.jp)

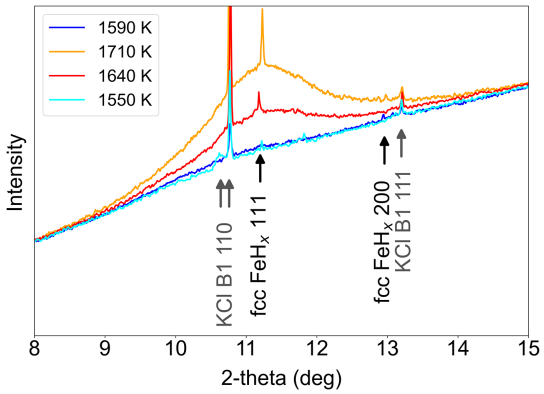

Figure 1 XRD patterns obtained from run #1 (spot #1-2) at 1.0 GPa (textured Fe peaks were masked to show diffuse scattering from molten Fe-H). The diffuse scattering signals indicative of melting appeared when sample temperature was increased from 1590 K (blue) to 1710 K (orange) and were still present when temperature was reduced to 1640 K (red). Then they disappeared upon cooling to 1550 K (cyan).

temperature to 1550 K (Fig. 1). The XRD data collected at 1710 K provided a strong diffuse scattering signal sufficient to determine the liquid density.

Similarly in run #2, we initially compressed the sample to 1.8 GPa and observed diffuse scattering upon increasing temperature from 1360 K at 2.1 GPa to 1440 K at 2.2 GPa, coexisting with fcc $FeH_{0.22}$ (spot #2-1). The diffuse scattering signals disappeared when decreasing temperature from 1440 K to 1310 K. We then increased temperature to 1530 K and collected XRD data providing a strong diffuse scattering signal. Subsequently the sample was further compressed to 2.7 GPa, and a fresh sample area was heated. The diffuse scattering signals appeared when increasing temperature from 1230 K at 3.0 GPa to 1380 K at 3.3 GPa (spot #2-2), coexisting with fcc $FeH_{0.29}$. We also collected an XRD pattern from this spot at 1670 K at 3.6 GPa for the analysis of liquid density.

These results locate the melting (solidus) curve of Fe-H in a pressure range from 1.0 to 3.3 GPa, showing that its melting temperature decreases monotonically from ambient pressure to ~3 GPa (Fig. 2), rather than a sudden reduction above ~2 GPa (Yagi and Hishinuma, 1995; Fukai *et al.*, 2003). Earlier studies attributed such melting temperature drop to a change in the subsolidus phase from body centred cubic (bcc) to fcc at ~2 GPa (Fukai *et al.*, 2003; Shibazaki *et al.*, 2014), but the present experiments demonstrate that liquid Fe-H coexists with fcc and the melting temperature is depressed already at 1.0 GPa.

We obtained hydrogen concentrations x in solid fcc FeH_x from XRD data collected at temperatures above the melting (solidus) curve and estimated liquid compositions at higher temperatures, where diffuse scattering signals were sufficiently intense for reliable density analysis (Fig. 3, Table S-1). The estimate of hydrogen abundance in the solids was based on the observed volume expansion of FeH_x with respect to Fe (see Experimental Methods in Supplementary Information). For the liquids, we first estimated the density of liquid FeH_x from diffuse scattering signals (Kuwayama *et al.*, 2020; Fu *et al.*, 2025). Subsequently the volume of liquid pure Fe at an identical P-T condition was calculated using its thermal equation of state (Kuwayama *et al.*, 2020). The volume expansion of liquid Fe-H relative to liquid pure Fe is attributed to hydrogen incorporation and converted to the hydrogen content. Hydrogen concentration in liquid FeH_x increased from x = 0.14 at 1.0 GPa to 0.48 at 3.6 GPa. The increase in the hydrogen abundance in liquid with increasing pressure is supported by the shift of the first peak position in structure factor $S(Q)$ (Fig. S-1). The first peak position decreased with increasing hydrogen concentration upon pressure increase. Since experiments were performed under H_2 saturated conditions, the resulting values correspond to the hydrogen solubility limit in liquid iron at each pressure.

Discussion

Melting phase diagram of Fe-H at low pressures. The present experiments demonstrate that the melting temperature in the Fe-H system decreases with increasing pressure from <1 GPa to ~3 GPa (Fig. 2). The magnitude of depression from the Fe melting curve is enhanced almost linearly with increasing pressure; ~240 K at 1 GPa, ~450 K at 2 GPa, and ~580 K at 3 GPa. This is explained by an increase in the solubility of hydrogen primarily into liquid iron with increasing pressure to ~3 GPa as evidenced by the XRD measurements (Fig. 3). Note that while the solubility of hydrogen into iron is enhanced with increasing pressure and temperature (Fukai and Suzuki, 1986), the pressure effect is much more significant in a limited temperature range relevant to this study.

The pressure evolution of the Fe-H melting phase diagram is illustrated in Figure S-2, in which we consider that the hydrogen solubility into liquid iron (excess hydrogen is present as

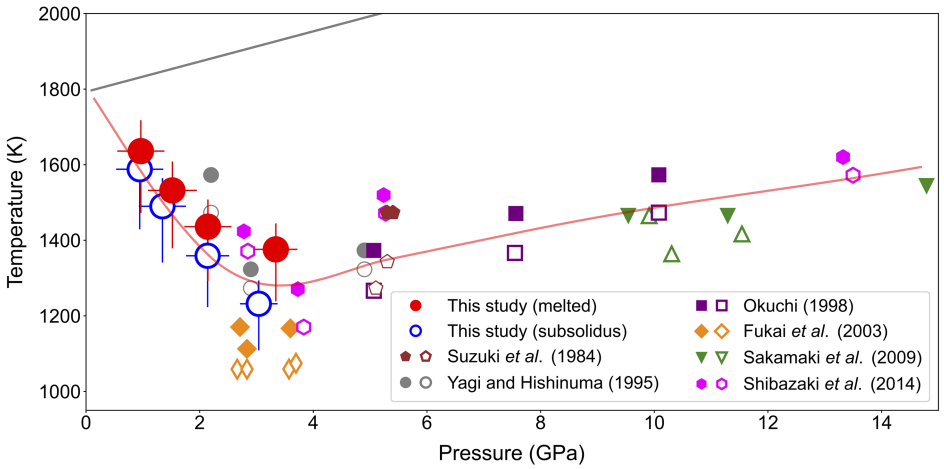

Figure 2 Melting curve of FeH_x ($0 < x < 1$) (red line). The grey line represents the melting curve of pure Fe (Strong *et al.*, 1973).

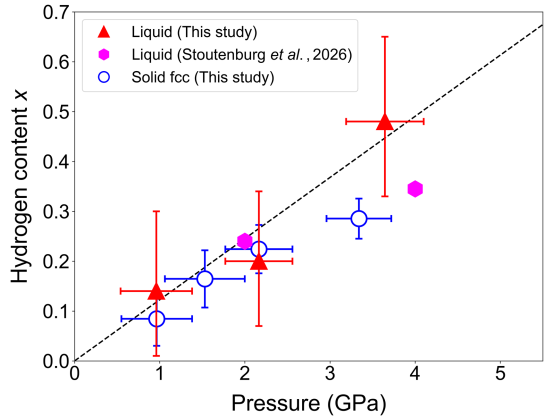

Figure 3 The hydrogen contents of fcc FeH_x immediately above the solidus and of liquid FeH_x at higher temperatures in this study. The theoretical predictions of those in liquid by Stoutenburg *et al.* (2026) at 1500 K are also shown. Considering a minimal solubility at 1 bar, the hydrogen solubility into liquid Fe is approximately linearly enhanced with pressure (broken line).

liquid H_2) increases approximately linearly with pressure to ~3 GPa, and accordingly the depression of eutectic temperature (above which metallic liquid is formed) from the Fe melting curve is also linearly enhanced with pressure. Earlier experiments reported that the Fe-H melting temperature conversely rises above ~3.5 GPa (Yagi and Hishinuma, 1995; Okuchi, 1998) (Fig. 2). It could be a consequence of a rapid increase in the hydrogen solubility into fcc Fe (Fig. S-2), which is inferred from the formation of stoichiometric FeH above that pressure at 300 K (Badding *et al.*, 1991).

Possible hydrogen abundance in the lunar core. The present experiments demonstrate the depression of melting temperature of iron by ~240 K even at 1.0 GPa in the presence of excess H_2, suggesting that liquid iron can incorporate hydrogen not at ambient pressure but certainly under lower pressures than previously thought. While recent planetary accretion and core formation modelling assumed that hydrogen is not soluble into core forming metals below 3 GPa (Tagawa *et al.*, 2021; Tsutsumi *et al.*, 2025), it is possible that metallic cores of small rocky bodies such as our moon also include some hydrogen. Indeed, the moon should have been covered with the protolunar disk gas, and therefore a lunar magma ocean (LMO) likely included a certain amount of water, most of which could have been later incorporated as hydrogen into core forming iron metals.

The depth of the LMO has been estimated to be 600 km, which explains the crustal thickness when all plagioclase crystallising from the LMO formed the crust (Charlier *et al.*, 2018). It is possible that the lunar core formation (in other words, core metal segregation from silicate) took place at its bottom under 2.8 GPa. On the other hand, Rai and van Westrenen (2014) found that core metal may have reached chemical equilibrium with silicate at 4.5 ± 0.5 GPa and 2163 K, which most likely matches the pressure at the core-mantle boundary. Furthermore, a more recent study suggested a much higher temperature of ~3200 K for the lunar core formation at 5 GPa in the case of an Fe-Ni core (Steenstra *et al.*, 2020). Here we consider the representative lunar core pressure to be 5 GPa. The present day core temperature may be about 1700 K (Garcia *et al.*, 2019; Kuskov *et al.*, 2021), which is well above the solidus temperature of the Fe-H system at 5 GPa (Fig. 2).

The solubility of hydrogen in liquid iron at 2.8 GPa or 5 GPa may limit its concentration in the lunar core. Considering that the reduction in Fe-H melting temperature with increasing pressure to ~3 GPa is primarily caused by the pressure induced enhancement of hydrogen solubility into liquid iron (see above), the hydrogen content in liquid iron at the melting (solidus) temperature will correspond to the solubility limit. Our results (Fig. 3) suggest that the hydrogen solubility limit in liquid iron may be x = 0.34 and 0.61 in FeH_x (0.6 and 1.1 wt. % H) at 2.8 and 5 GPa, respectively.

As an independent estimate, we can also calculate the possible hydrogen content in the lunar core based on its metal-silicate partitioning under core formation conditions. Water concentration in the bulk silicate moon (BSM) has been estimated from the analyses of lunar volcanic glasses. Hauri *et al.* (2015) found that the BSM is similar in highly volatile element composition to the depleted MORB source mantle of the Earth, giving 133–292 μg/g H_2O in the BSM. The magma ocean models by Elkins-Tanton and Grove (2011) demonstrated that the LMO should have contained 100 to >1000 μg/g water when the later melting source region for such volcanic glasses includes 10 to 200 μg/g water. Also, Lin *et al.* (2020) argued that the lunar crustal thickness (the amount of plagioclase) is controlled by water abundance in the LMO, which may be ~300 μg/g H_2O if the LMO was 700 km deep. Hydrogen incorporation from silicate melt into core forming metals has been investigated under high pressures (Clesi *et al.*, 2018; Malavergne *et al.*, 2019; Tagawa *et al.*, 2021; Tsutsumi *et al.*, 2025). Under plausible conditions of the lunar core formation of 2.8 GPa, 2163 K, and oxygen fugacity relative to the iron-wüstite buffer ΔIW = −2 (Rai and van Westrenen, 2014), the partition coefficient of hydrogen $D_H^{metal/silicate}$ is 1.11 × 10^2 (molar basis) according to Tsutsumi *et al.* (2025) (Fig. S-3). We also obtained $D_H^{metal/silicate}$ = 1.05 × 10^2 at 5 GPa and 2200 K (based on the liquidus temperature estimate by Rai and van Westrenen, 2014) and 1.85 × 10^2 at 3200 K (from the high temperature core formation model by Steenstra *et al.*, 2020). Even with 300 μg/g H_2O (34 μg/g H) in the LMO (Lin *et al.*, 2020), the metal-silicate partitioning predicts ~0.3 wt. % H in the lunar core when it occurred at both 2.8 GPa/2163 K and 5 GPa/2200 K and ~0.6 wt. % H at 5 GPa/3200 K. If instead the LMO included 1000 μg/g H_2O (111 μg/g H) at the time of the core formation, core hydrogen concentration could be as high as ~1.1 wt. % and ~1.8 wt. % H at respective core formation conditions (see Table S-2, and Calculations of Metal-Silicate Partitioning of Hydrogen in Supplementary Information).

Is hydrogen a major light element in the lunar core? The density of the lunar core has been modelled to be 4200–5200 kg/m^3 by Garcia *et al.* (2019) and 5560–6070 kg/m^3 by Viswanathan *et al.* (2019) assuming homogeneous liquid core. The more recent work by Kuskov *et al.* (2021) proposed a higher density range of 6200–7000 kg/m^3 for the liquid core, considering the outer liquid and inner solid cores (Fig. 4).

We calculated the density of liquid Fe-H by considering the volume expansion due to the incorporation of hydrogen atoms into iron (Fig. 4). The maximum 0.6–1.1 wt. % H in the lunar core based on the hydrogen solubility limit reconciles within uncertainty the lunar liquid core density deficit estimated by Kuskov *et al.* (2021) with hydrogen alone, although it is not enough for the lower densities proposed earlier by Garcia *et al.* (2019) and Viswanathan *et al.* (2019). Furthermore, if the metal-silicate chemical equilibrium was attained at the bottom of the LMO, our estimate of 0.3–1.8 wt. % H in the core can explain the observed density within its large uncertainty (Kuskov *et al.*, 2021). It is noted, however, that these estimates do not exclude the possible coexistence of other light elements such as carbon and sulfur in the lunar core.

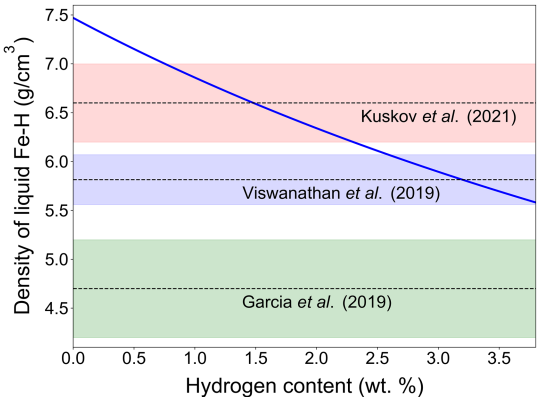

Figure 4 Density of liquid FeH_x as a function of hydrogen concentration at 5 GPa and 1700 K. The density of liquid pure Fe is from Kuwayama *et al.* (2020), and density reduction with increasing hydrogen content is calculated with ΔV_H = 2.22 Å^3. The solubility limit of hydrogen into liquid iron is estimated to be 0.6–1.1 wt. % at the base of the LMO and at the core-mantle boundary. Metal-silicate partitioning suggests 0.3–1.8 wt. % H in the core. These amounts of hydrogen account for the lunar core density estimated by Kuskov *et al.* (2021), while other light elements such as sulfur and carbon are required for earlier estimates by Garcia *et al.* (2019) and Viswanathan *et al.* (2019).

Not only density but also sound velocity provides an important constraint on the lunar core composition. Fu *et al.* (2025) based on experiments above 27 GPa showed that hydrogen incorporation increases the velocity of liquid Fe. In contrast, Nishida *et al.* (2020) suggested that sulfur strongly reduces the velocity of liquid iron under lunar core conditions. Thus, the relatively low compressional wave velocity (V_P) inferred for the lunar core (Weber *et al.*, 2011) may require light elements such as sulfur. We note, however, that the sound velocity of Fe-H liquids remains poorly known at the lunar core pressure. Recent theoretical calculations found non-ideal mixing behaviour of Fe-H liquids under the lunar core pressures (Stoutenburg *et al.*, 2026), possibly lowering their sound velocity. Indeed, the calculations by van Driel *et al.* (2025) showed that V_P is faster for liquid Fe-H than for pure Fe above 20 GPa but the difference is smaller at lower pressures, suggesting a possibility that hydrogen reduces the sound velocity of liquid Fe at 5 GPa.

These results suggest that hydrogen could be, at least, a major light element in the lunar core. Sulfur and carbon have previously been proposed to be important lunar core light elements, but we note that their solubilities into solid iron coexisting with liquid alloy are limited only to <0.5 wt. % S and 1.5 wt. % C at 5 GPa (Li *et al.*, 2001; Fei and Brosh, 2014). This indicates that if the lunar solid inner core also exhibits a definite density deficit with respect to iron beyond the solubilities of sulfur and carbon, hydrogen is certainly an important lunar core light element.

Acknowledgements

We thank two anonymous reviewers whose comments were valuable to improve the manuscript. H. Kadobayashi and N. Hirao are acknowledged for their assistance in the synchrotron experiments and high-pressure gas loading at SPring-8 (proposals no. 2023B0306, 2025A1133 and 2025B1212). Discussion with S. Yokoo was helpful. This work was supported by the JSPS grant 21H04968 and 26H02080 to K. Hirose.

Editor: Raul O.C. Fonseca

Additional Information

Supplementary Information accompanies this letter at https://www.geochemicalperspectivesletters.org/article2633.

Cite this letter as: Takeshita, J., Hirose, K., Fu, S., Sakai, F., Hikosaka, K. (2026) Fe-H melting curve below 3 GPa: implications for hydrogen in the lunar core. *Geochem. Persp. Let.* 41, 53–57. https://doi.org/10.7185/geochemlet.2633

References

Badding, J.V., Hemley, R.J., Mao, H.K. (1991) High-pressure chemistry of hydrogen in metals: in situ study of iron hydride. *Science* 253, 421–424. https://doi.org/10.1126/science.253.5018.421

Charlier, B., Grove, T.L., Namur, O., Holtz, F. (2018) Crystallization of the lunar magma ocean and the primordial mantle–crust differentiation of the Moon. *Geochimica et Cosmochimica Acta* 234, 50–69. https://doi.org/10.1016/j.gca.2018.05.006

Clesi, V., Bouhifd, M.A., Bolfan-Casanova, N., Manthilake, G., Schiavi, F., Raepsaet, C., Bureau, H., Khodja, H., Andrault, D. (2018) Low hydrogen contents in the cores of terrestrial planets. *Science Advances* 4, e1701876. https://doi.org/10.1126/sciadv.1701876

Elkins-Tanton, L.T., Grove, T.L. (2011) Water (hydrogen) in the lunar mantle: results from petrology and magma ocean modeling. *Earth and Planetary Science Letters* 307, 173–179. https://doi.org/10.1016/j.epsl.2011.04.027

Fei, Y., Brosh, E. (2014) Experimental study and thermodynamic calculations of phase relations in the Fe–C system at high pressure. *Earth and Planetary Science Letters* 408, 155–162. https://doi.org/10.1016/j.epsl.2014.09.044

Fu, S., Hirose, K., Yokoo, S., Sakai, F., Oka, K. (2025) Hydrogen in the Earth's outer core from density measurements of liquid Fe-H up to 102 GPa and 4,100 K. *Journal of Geophysical Research: Solid Earth* 130, e2025JB031934. https://doi.org/10.1029/2025JB031934

Fukai, Y., Suzuki, T. (1986) Iron-water reaction under high pressure and its implication in the evolution of the Earth. *Journal of Geophysical Research: Solid Earth* 91, 9222–9230. https://doi.org/10.1029/JB091iB09p09222

Fukai, Y., Mori, K., Shinomiya, H. (2003) The phase diagram and superabundant vacancy formation in Fe–H alloys under high hydrogen pressures. *Journal of Alloys and Compounds* 348, 105–109. https://doi.org/10.1016/S0925-8388(02)00806-X

Garcia, R.F., Khan, A., Drilleau, M., Margerin, L., Kawamura, T., Sun, D., Wieczorek, M.A., Rivoldini, A., Nunn, C., Weber, R.C., Marusiak, A.G., Lognonné, P., Nakamura, Y., Zhu, P. (2019) Lunar seismology: an update on interior structure models. *Space Science Reviews* 215, 50. https://doi.org/10.1007/s11214-019-0613-y

Hauri, E.H., Saal, A.E., Rutherford, M.J., Van Orman, J.A. (2015) Water in the Moon's interior: truth and consequences. *Earth and Planetary Science Letters* 409, 252–264. https://doi.org/10.1016/j.epsl.2014.10.053

Iizuka-Oku, R., Yagi, T., Gotou, H., Okuchi, T., Hattori, T., Sano-Furukawa, A. (2017) Hydrogenation of iron in the early stage of Earth's evolution. *Nature Communications* 8, 14096. https://doi.org/10.1038/ncomms14096

Ikuta, D., Ohtani, E., Sano-Furukawa, A., Shibazaki, Y., Terasaki, H., Yuan, L., Hattori, T. (2019) Interstitial hydrogen atoms in face-centered cubic iron in the Earth's core. *Scientific Reports* 9, 7108. https://doi.org/10.1038/s41598-019-43601-z

Jing, Z., Wang, Y., Kono, Y., Yu, T., Sakamaki, T., Park, C., Rivers, M.L., Sutton, S.R., Shen, G. (2014) Sound velocity of Fe–S liquids at high pressure: implications for the Moon's molten outer core. *Earth and Planetary Science Letters* 396, 78–87. https://doi.org/10.1016/j.epsl.2014.04.015

Kuskov, O.L., Kronrod, E.V., Matsumoto, K., Kronrod, V.A. (2021) Physical properties and internal structure of the central region of the Moon. *Geochemistry International* 59, 1018–1037. https://doi.org/10.1134/S0016702921110069

Kuwayama, Y., Morard, G., Nakajima, Y., Hirose, K., Baron, A.Q.R., Kawaguchi, S.I., Tsuchiya, T., Ishikawa, D., Hirao, N., Ohishi, Y. (2020) Equation of state of liquid iron under extreme conditions. *Physical Review Letters* 124, 165701. https://doi.org/10.1103/PhysRevLett.124.165701

Li, J., Fei, Y., Mao, H.K., Hirose, K., Shieh, S.R. (2001) Sulfur in the Earth's inner core. *Earth and Planetary Science Letters* 193, 509–514. https://doi.org/10.1016/S0012-821X(01)00521-0

Lin, Y., Hui, H., Xia, X., Shang, S., van Westrenen, W. (2020) Experimental constraints on the solidification of a hydrous lunar magma ocean. *Meteoritics & Planetary Science* 55, 207–230. https://doi.org/10.1111/maps.13425

Machida, A., Saitoh, H., Hattori, T., Sano-Furukawa, A., Funakoshi, K.-i., Sato, T., Orimo, S.-i., Aoki, K. (2019) Hexagonal close-packed iron hydride behind the conventional phase diagram. *Scientific Reports* 9, 12290. https://doi.org/10.1038/s41598-019-48817-7

Malavergne, V., Bureau, H., Raepsaet, C., Gaillard, F., Poncet, M., Surblé, S., Sifré, D., Shcheka, S., Fourdrin, C., Deldicque, D., Khodja, H. (2019) Experimental constraints on the fate of H and C during planetary core-mantle differentiation. Implications for the Earth. *Icarus* 321, 473–485. https://doi.org/10.1016/j.icarus.2018.11.027

Mita, S., Tagawa, S., Hirose, K., Ikuta, N. (2025) Fe-FeH eutectic melting curve and the estimates of Earth's core temperature and composition. *Journal of Geophysical Research: Solid Earth* 130, e2024JB029283. https://doi.org/10.1029/2024JB029283

Nishida, K., Shibazaki, Y., Terasaki, H., Higo, Y., Suzuki, A., Funamori, N., Hirose, K. (2020) Effect of sulfur on sound velocity of liquid iron under Martian core conditions. *Nature Communications* 11, 1954. https://doi.org/10.1038/s41467-020-15755-2

Okuchi, T. (1998) The melting temperature of iron hydride at high pressures and its implications for the temperature of the Earth's core. *Journal of Physics: Condensed Matter* 10, 11595–11598. https://doi.org/10.1088/0953-8984/10/49/052

Rai, N., van Westrenen, W. (2014) Lunar core formation: new constraints from metal–silicate partitioning of siderophile elements. *Earth and Planetary Science Letters* 388, 343–352. https://doi.org/10.1016/j.epsl.2013.12.001

Sakamaki, K., Takahashi, E., Nakajima, Y., Nishihara, Y., Funakoshi, K., Suzuki, T., Fukai, Y. (2009) Melting phase relation of FeH_x up to 20 GPa: implication for the temperature of the Earth's core. *Physics of the Earth and Planetary Interiors* 174, 192–201. https://doi.org/10.1016/j.pepi.2008.05.017

Shibazaki, Y., Terasaki, H., Ohtani, E., Tateyama, R., Nishida, K., Funakoshi, K.-i., Higo, Y. (2014) High-pressure and high-temperature phase diagram for $Fe_{0.9}Ni_{0.1}$–H alloy. *Physics of the Earth and Planetary Interiors* 228, 192–201. https://doi.org/10.1016/j.pepi.2013.12.013

Steenstra, E.S., Lin, Y., Rai, N., Jansen, M., van Westrenen, W. (2017) Carbon as the dominant light element in the lunar core. *American Mineralogist* 102, 92–97. https://doi.org/10.2138/am-2017-5727

Steenstra, E.S., Berndt, J., Klemme, S., Fei, Y., van Westrenen, W. (2020) A possible high-temperature origin of the Moon and its geochemical consequences. *Earth and Planetary Science Letters* 538, 116222. https://doi.org/10.1016/j.epsl.2020.116222

Stoutenburg, E.R., Caracas, R., Campbell, A.J. (2026) Immiscibility between hydrogen and molten iron in planetary cores. *Earth and Planetary Science Letters* 678, 119851. https://doi.org/10.1016/j.epsl.2026.119851

Strong, H.M., Tuft, R.E., Hanneman, R.E. (1973) The iron fusion curve and γ-δ-l triple point. *Metallurgical Transactions* 4, 2657–2661. https://doi.org/10.1007/BF02644272

Suzuki, T., Akimoto, S.-i., Fukai, Y. (1984) The system iron-enstatite-water at high pressures and temperatures—formation of iron hydride and some geophysical implications. *Physics of the Earth and Planetary Interiors* 36, 135–144. https://doi.org/10.1016/0031-9201(84)90014-1

Tagawa, S., Sakamoto, N., Hirose, K., Yokoo, S., Hernlund, J., Ohishi, Y., Yurimoto, H. (2021) Experimental evidence for hydrogen incorporation into Earth's core. *Nature Communications* 12, 2588. https://doi.org/10.1038/s41467-021-22035-0

Tsutsumi, Y., Sakamoto, N., Hirose, K., Mita, S., Yokoo, S., Hsu, H., Yurimoto, H. (2025) Origin of Earth's hydrogen and carbon constrained by their core-mantle partitioning and bulk Earth abundance. *Nature Communications* 16, 10038. https://doi.org/10.1038/s41467-025-65729-5

van Driel, J., Vočadlo, L., Brodholt, J. (2025) Thermodynamics of Fe-S-O-C-H liquids: implications for the Martian core. *Earth and Planetary Science Letters* 668, 119540. https://doi.org/10.1016/j.epsl.2025.119540

Viswanathan, V., Rambaux, N., Fienga, A., Laskar, J., Gastineau, M. (2019) Observational constraint on the radius and oblateness of the lunar core-mantle boundary. *Geophysical Research Letters* 46, 7295–7303. https://doi.org/10.1029/2019GL082677

Weber, R.C., Lin, P.-Y., Garnero, E.J., Williams, Q., Lognonné, P. (2011) Seismic detection of the lunar core. *Science* 331, 309–312. https://doi.org/10.1126/science.1199375

Yagi, T., Hishinuma, T. (1995) Iron hydride formed by the reaction of iron, silicate, and water: implications for the light element of the Earth's core. *Geophysical Research Letters* 22, 1933–1936. https://doi.org/10.1029/95GL01792

Zhao, B., Morard, G., Boulard, E., Boccato, S., Siersch, N.C., Rivoldini, A., Guignot, N., Henry, L., King, A., Zurkowski, C., Fei, Y., Antonangeli, D. (2023) Local structure and density of liquid Fe-C-S alloys at Moon's core conditions. *Journal of Geophysical Research: Planets* 128, e2022JE007577. https://doi.org/10.1029/2022JE007577

Fe-H melting curve below 3 GPa: Implications for hydrogen in the lunar core

J. Takeshita, K. Hirose, S. Fu, F. Sakai, K. Hikosaka

Supplementary Information

The Supplementary Information includes:

- Experimental Methods
- Estimates of the Hydrogen Content in Liquid Iron
- Calculations of Metal-Silicate Partitioning of Hydrogen
- Tables S-1 and S-2
- Figures S-1 to S-4
- Supplementary Information References

Experimental Methods

High-pressure and -temperature (*P-T*) experiments were conducted in a laser-heated diamond-anvil cell (LH-DAC) using diamond anvils with flat 800 μm culet (we can precisely control experimental pressure by using anvils with such large culet size). The anvil surface was coated with a 500 nm-thick Ti layer by sputtering in order to prevent hydrogen penetration into diamonds (Ohta *et al.*, 2015). We loaded a pure Fe foil (Toho Zinc, >99.999% purity) with a thickness of approximately 20 μm into a hole at the centre of a pre-indented Re gasket, leaving space for hydrogen. Pressure markers of KCl and a ruby ball were placed beneath the Fe foil. Subsequently the DAC was placed in an oven maintained at 120 °C for 1 hour in order to remove moisture from the KCl. Supercritical hydrogen fluid was introduced into the sample chamber using a high-pressure gas apparatus (PRETECH Co., Ltd) at SPring-8. The high-pressure vessel and gas line were evacuated for 5 minutes and subsequently purged four times with H_2 gas prior to loading into the DAC. The presence of H_2 molecules was confirmed by Raman spectra. The sample was then compressed to a target pressure, with monitoring pressure by the ruby ball.

We obtained X-ray diffraction (XRD) data at the beamline BL10XU of SPring-8. The incident X-ray beam was monochromatized to ~30 keV and focused to 6 μm in diameter (full-width at half maximum). XRD patterns were collected using a flat panel X-ray detector (Varex Imaging, XRD1611CP3). The obtained 2D XRD images were converted into 1D patterns using IPAnalyzer software (Seto *et al.*, 2010), and phase identification and unit-cell volume derivation were performed. We heated the Fe + H_2 sample from both sides

using a couple of 100 W single-mode Yb fibre lasers (SPI Lasers Co. Ltd.). The laser spot size was approximately 50 μm in diameter. Using visible fluorescence that appeared upon irradiating X-ray onto the KCl medium, the laser beams from both sides were adjusted to be coaxial with the X-ray beam. The laser power output was increased stepwise, and the XRD spectrum and temperature were collected/measured each time. The laser power output was maintained for several tens of seconds at each step. We measured temperature at the iron sample surface by a spectro-radiometric method (Hirao *et al.*, 2020). The average within the 6 μm area probed by the XRD beam was adopted as the sample temperature. While Mita *et al.* (2025) considered 5% uncertainty for both the upper and lower bounds, we employed a much thicker (20 μm) iron sample in this study, which causes larger temperature variations in axial direction toward the sample inside (hottest at the surface and colder inside). The earlier laser-heated DAC experiments by Tateno *et al.* (2018) demonstrated an axial temperature gradient of about 18 K/μm in their 9.4 μm thick Fe sample (see their Fig. 1b), which corresponds to 0.7–0.8% of the surface temperature (2350 K) per μm. We therefore consider additional −7% (total −12% for the lower bound) temperature variations from the surface to the core (centre) in our sample. Pressure under high temperature was determined from the lattice volume of the B1 or B2 phase of KCl and their thermal equations of state (EoSs, Walker *et al.*, 2002; Tateno *et al.*, 2019). The pressure error was evaluated by considering uncertainties in the lattice volume and temperature of the KCl pressure marker, which was in contact with a diamond anvil on one side and covered with hydrogen on the other side. We consider that the temperature of the KCl ranged from 300 K to an effective temperature that is given by Campbell *et al.* (2009) as $(3 \times T_{\mathrm{measured}} + 300) / 4$, in which T_{measured} represents the measured iron sample temperature (or the melting temperature of KCl, whichever was lower). The resulting pressure uncertainty was dominated by the uncertainty in the estimated KCl temperature.

It is known that hydrogen escapes from iron when it turns to the bcc phase (*e.g.,* Iizuka-Oku *et al.*, 2017; Tagawa *et al.*, 2021). It is necessary to determine hydrogen concentration x in fcc FeH_x at high P-T because it transforms into the bcc phase upon quenching temperature in the pressure range of the present experiments. The hydrogen content is calculated as:

$$x = \frac{V_{\mathrm{FeH}_x} - V_{\mathrm{Fe}}}{\Delta V_{\mathrm{H}}} \tag{S-1}$$

where V represents the volume per chemical formula (half of the unit-cell volume of fcc). V_{Fe} for the fcc phase was derived from the EoS of pure fcc-Fe reported by Tsujino *et al.* (2013). ΔV_{H} (= 2.22 Å^3), the volume expansion upon incorporation of one hydrogen atom into the Fe lattice, was adopted from the value for fcc FeH_x at 4–12 GPa and about 1000 K reported by Ikuta *et al.* (2019).

Estimates of the Hydrogen Content in Liquid Iron

The amount of hydrogen in liquid iron could not be obtained in the manner described above, because the liquids crystallized into bcc Fe upon quenching temperature, which does not incorporate hydrogen into its lattice. Alternatively, we obtained the density of liquid FeH_x and then determined x considering ΔV_{H}. First, liquid density was calculated from the diffuse scattering signal in XRD data by non-iterative extension procedures described by Kuwayama *et al.* (2020), which were built on earlier diffuse-scattering analyses for liquid density determination, including Eggert *et al.* (2002) (Fig. S-4). High-pressure XRD measurements in a DAC always have a limitation on the range of momentum transfer Q (up to Q_{max}) because of a geometrical constraint, which leads to artificial oscillations in distribution function $F(r)$ and pair distribution function $g(r)$. Indeed, no atoms can exist at distances shorter than the nearest-neighbour atomic distance ($r < r_{\mathrm{min}}$), meaning that the local density must be zero. We therefore complemented the data to satisfy such physical requirement, $g(r) = 0$ at $r < r_{\mathrm{min}}$ (in other words, for $F(r)$ to exhibit a straight line with a slope of $-4\pi\rho r$, where ρ is the average atomic number density). In this procedure, only the unmeasured high-Q part beyond Q_{max} was supplemented.

For each liquid density measurement, an XRD pattern collected immediately below the melting temperature at the same sample position was used as the background. The liquid diffuse scattering signal was obtained as:

$$I_{\mathrm{liq}}(Q) = I_{\mathrm{melt}}(Q) - sI_{\mathrm{bk}}(Q) \quad \text{(S-2)}$$

where $I_{\mathrm{melt}}(Q)$ and $I_{\mathrm{bk}}(Q)$ are the XRD patterns collected above and below the melting temperature, respectively, and s is a scale factor accounting for small differences in the incident X-ray intensity and background level. Note that both patterns were collected through the identical diamond anvils and along the same X-ray path. Therefore, subtracting the unmelted pattern from the melting pattern should largely remove scattering contributions common to both measurements, including Compton scattering from the diamonds. The resulting diffuse intensity was then normalized using the composition-dependent factor of the FeH_x liquid, $\langle f \rangle$. Because hydrogen contributes negligibly to the X-ray scattering signal, $\langle f \rangle$ was approximated by the Fe atomic form factor, $f_{\mathrm{Fe}(Q)}$. Subsequently $S(Q)$ of liquid Fe-H is calculated as:

$$S(Q) = \frac{\alpha_{\mathrm{N}} I(Q)}{f^2_{\mathrm{Fe}(Q)}} \quad \text{(S-3)}$$

where α_{N} is a normalization factor.

The density was determined by searching for a parameter set that minimizes the deviation of $g(r)$ from zero at $r < r_{\mathrm{min}}$. In the fitting, r_{min}, the scale factor s, normalization factor α_{N}, density ρ, and Q_{max} were allowed to vary together. The derived density typically includes ±~2% uncertainty. More technical details are found in Kuwayama *et al.* (2020) and Fu *et al.* (2025), who derived the densities of liquids Fe and FeH_x, respectively. The hydrogen content in liquid FeH_x is then estimated from the density difference from liquid pure Fe using $\Delta V_{\mathrm{H}} = 2.22$ Å^3 from Ikuta *et al.* (2019). The density of liquid Fe is from the EoS by Kuwayama *et al.* (2020). Although the liquid density measurements by Kuwayama *et al.* (2020) were conducted at 21.5 GPa and higher pressures, their EoS well reproduces the known density of liquid Fe at 1 bar and its sound velocity data below 5.8 GPa, despite these low-pressure data not being used in obtaining their EoS. According to the EoSs of liquid Fe by Kuwayama *et al.* (2020) and liquid Fe-H by Fu *et al.* (2025), the densities of Fe and $FeH_{0.3}$ are 7.47 and 7.13 g/cm^3, respectively, at 5 GPa and 1700 K, indicating $\Delta V_{\mathrm{H}} = 2.17$ Å^3, which matches the value by Ikuta *et al.* (2019). The uncertainty in x was calculated by first-order propagation of the uncertainties in pressure, temperature, Fe number density, and ΔV_{H}.

Calculations of Metal-Silicate Partitioning of Hydrogen

The hydrogen content in the lunar core was calculated using $D_{\mathrm{H}}^{\mathrm{metal/silicate}}$ (molar basis) reported by Tsutsumi *et al.* (2025). We adopted the lunar primitive upper mantle composition from Longhi (2003) for the LMO composition and 0 to 7 wt. % S in the core following Jing *et al.* (2014). Note that Tsutsumi *et al.* (2025)'s $D_{\mathrm{H}}^{\mathrm{metal/silicate}}$ values were obtained by considering that hydrogen does not have a colligative property in iron solvent since small H atoms are incorporated into liquid Fe interstitially and therefore the activity of element i in metal is approximated as:

$$x_i' = \frac{N_i}{\sum_{k \neq \mathrm{H}} N_k} \quad \text{(S-4)}$$

Supplementary Tables

Table S-1 Experimental results on melting and hydrogen content x in FeH_x.

Run		#1		#2	
Spot		#1-1	#1-2	#2-1	#2-2
Subsolidus	P [GPa]	1.3(4)	1.0(4)	2.1(4)	3.0(3)
	T [K]	$1490(^{+70}_{-180})$	$1590(^{+80}_{-190})$	$1360(^{+70}_{-160})$	$1230(^{+60}_{-150})$
Right above solidus	P [GPa]	1.5(5)	1.0(4)	2.2(4)	3.3(4)
	T [K]	$1530(^{+80}_{-180})$	$1640(^{+80}_{-200})$	$1440(^{+70}_{-170})$	$1380(^{+70}_{-170})$
	x (fcc)	0.16(5)	0.08(6)	0.22(5)	0.29(4)
Liquid density measurements	P [GPa]	–	1.0(4)	2.2(4)	3.6(4)
	T [K]	–	$1710(^{+90}_{-210})$	$1530(^{+80}_{-180})$	$1670(^{+80}_{-200})$
	ρ (liquid) [g/cm^3]	–	7.03(12)	7.12(14)	6.87(12)
	x (liquid)	–	$0.14(^{+16}_{-13})$	$0.20(^{+14}_{-13})$	$0.48(^{+17}_{-15})$

Table S-2 Partitioning of H under representative core-formation conditions and resulting its abundance in the lunar core.

Pressure (GPa)	Temperature (K)	$D_H^{metal/silicate}$	Core H (wt. %) for LMO H_2O = 300 µg/g	Core H (wt. %) for LMO H_2O = 1000 µg/g
2.8	2163	1.11×10^2	0.3	1.1
5.0	2200	1.05×10^2	0.3	1.1
5.0	3200	1.85×10^2	0.6	1.8

Supplementary Figures

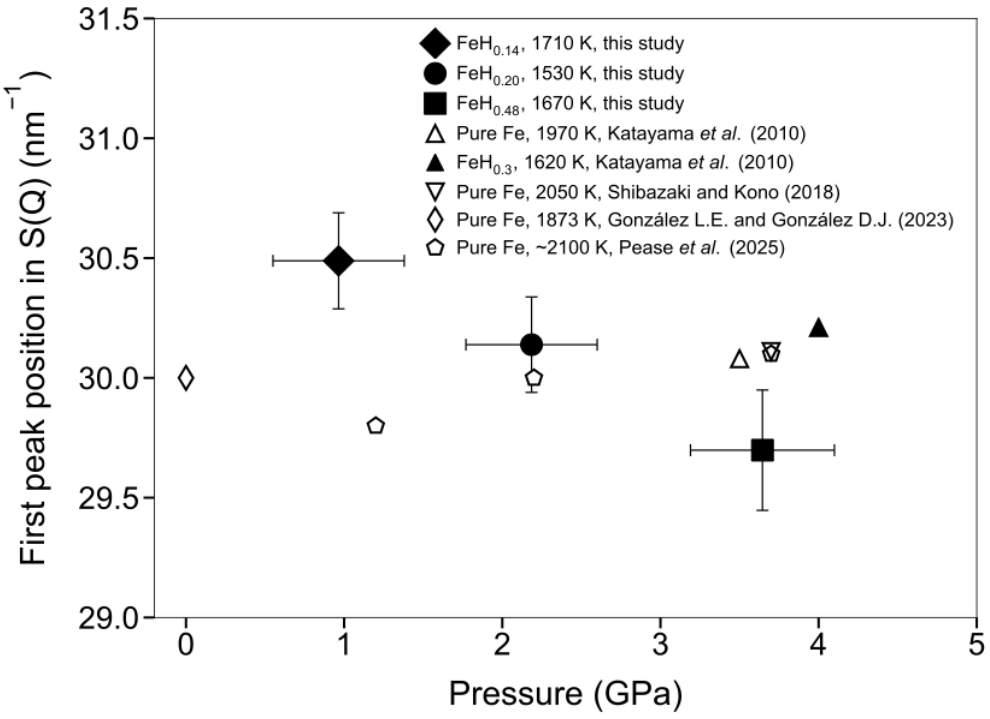

Figure S-1 The first peak position in the structure factor $S(Q)$. The observed shift for liquid FeH_x indicates a larger volume and thus higher hydrogen concentration with increasing pressure from 1.0 to 3.6 GPa. Note that the $S(Q)$ profile of this study is merely the one for the purpose of yielding the correct $g(r)$ and $F(r)$ (see Fig. S-4).

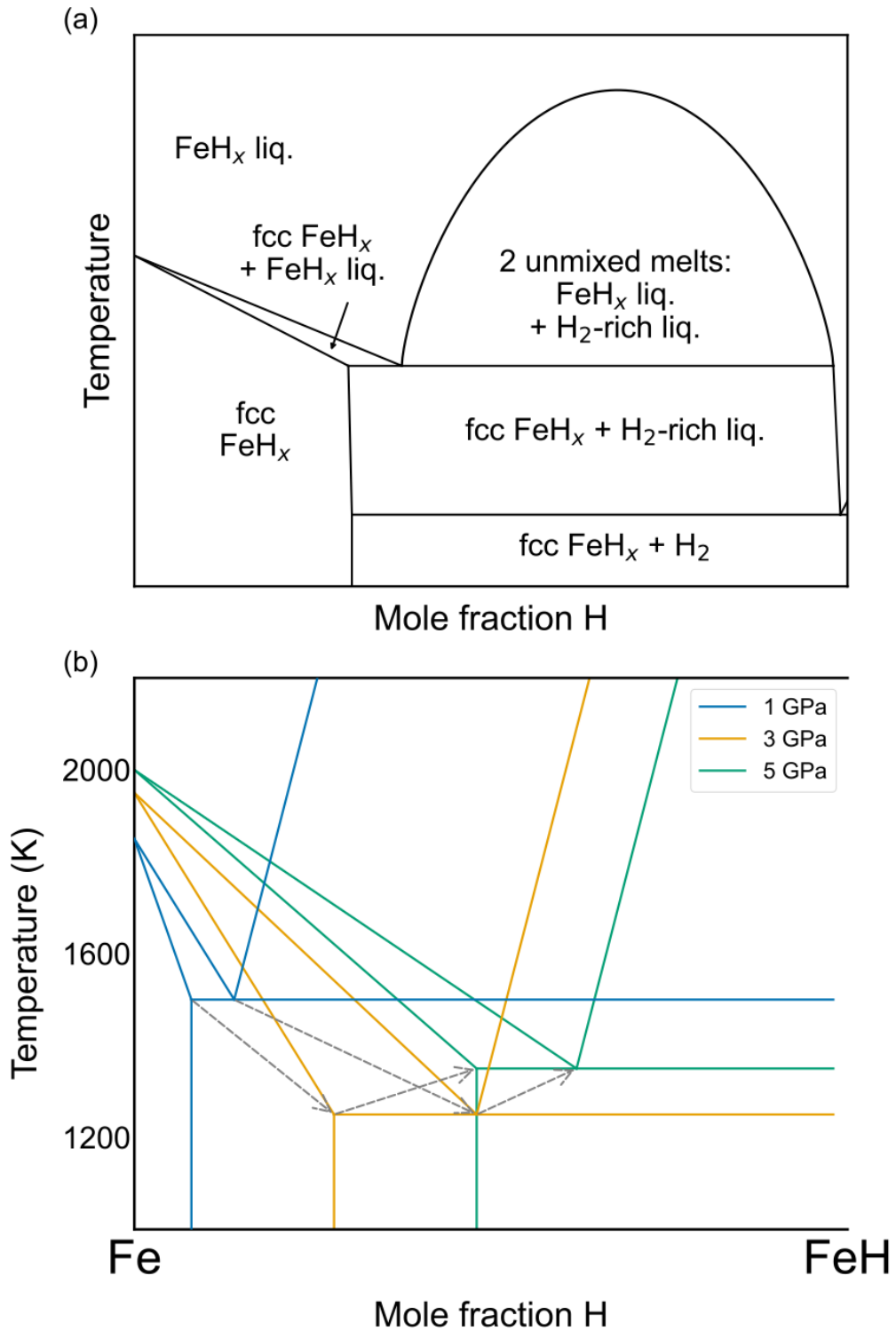

Figure S-2 **(a)** Schematic phase diagram between Fe and H_2 under pressure (less than ~10 GPa) based on Tagawa *et al.* (2022) and Stoutenburg *et al.* (2026). **(b)** The Fe-rich portion of the Fe-H phase diagram, showing the enhanced solubilities of hydrogen in solid and liquid iron and the changes in solidus temperature with increasing pressure from 1 to 5 GPa.

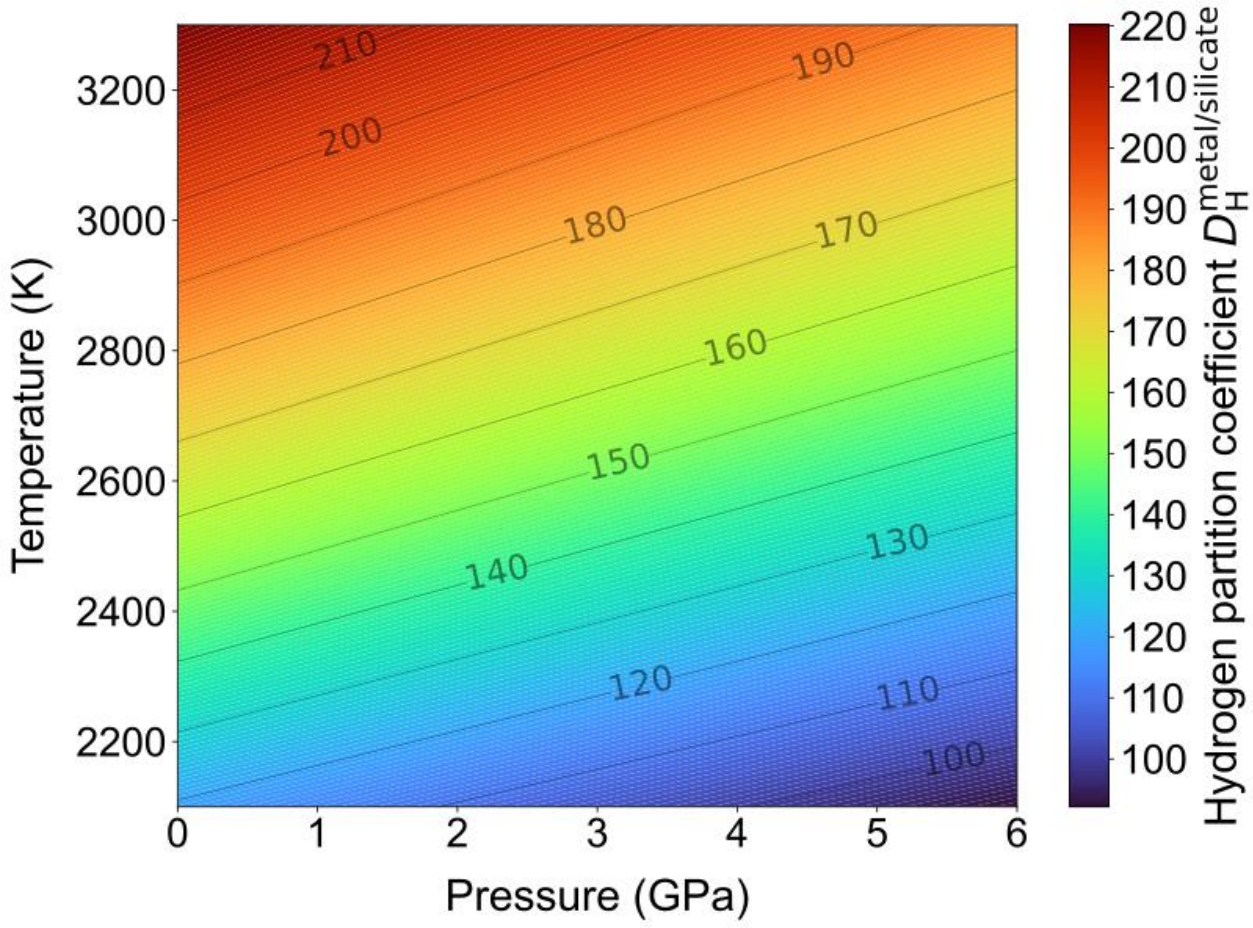

Figure S-3 Metal-silicate partition coefficient of hydrogen ($D_H^{metal/silicate}$, molar basis) as functions of pressure and temperature from Tsutsumi *et al.* (2025), considering ΔIW = −2 (Rai and van Westrenen, 2014) and carbon-free metal composition.

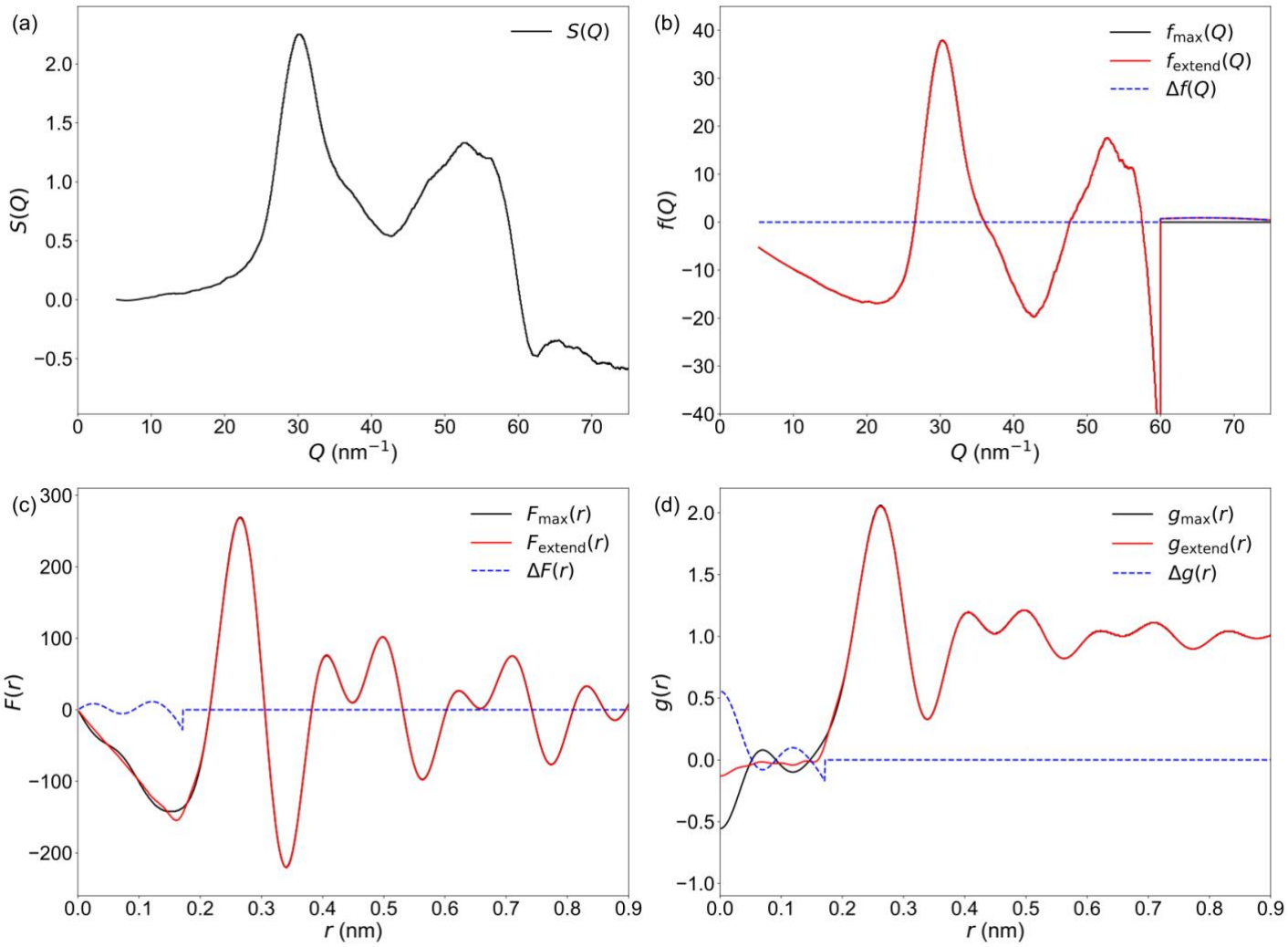

Figure S-4 Determination of liquid density from diffuse scattering using the analytical method developed by Kuwayama *et al.* (2020). **(a)** The structure factor $S(Q)$, **(b)** reduced interference function $f(Q)$, **(c)** distribution function $F(r)$, and **(d)** radial distribution function $g(r)$ (Q is momentum transfer). The black lines represent raw data, and the blue broken lines show complements added for the physical requirement that no atoms can exist at distances shorter than the nearest-neighbour atomic distance [$g(r) = 0$ at $r < r_{min}$]. With such data complements (red lines), $F(r)$ exhibits a straight line with a slope of $-4\pi\rho r$ (ρ is average atomic number density). See the supplemental text for details.

Supplementary Information References

Campbell, A.J., Danielson, L., Righter, K., Seagle, C.T., Wang, Y., Prakapenka, V.B. (2009) High pressure effects on the iron–iron oxide and nickel–nickel oxide oxygen fugacity buffers. *Earth and Planetary Science Letters* 286, 556–564. https://doi.org/10.1016/j.epsl.2009.07.022

Eggert, J.H., Weck, G., Loubeyre, P., Mezouar, M. (2002) Quantitative structure factor and density measurements of high-pressure fluids in diamond anvil cells by x-ray diffraction: argon and water. *Physical Review B* 65, 174105. https://doi.org/10.1103/PhysRevB.65.174105

Fu, S., Hirose, K., Yokoo, S., Sakai, F., Oka, K. (2025) Hydrogen in the Earth's outer core from density measurements of liquid Fe-H up to 102 GPa and 4,100 K. *Journal of Geophysical Research: Solid Earth* 130, e2025JB031934. https://doi.org/10.1029/2025JB031934

González, L.E., González, D.J. (2023) Structure and dynamics in liquid iron at high pressure and temperature: a first principles study. *Journal of Geophysical Research: Solid Earth* 128, e2022JB025119. https://doi.org/10.1029/2022JB025119

Hirao, N., Kawaguchi, S.I., Hirose, K., Shimizu, K., Ohtani, E., Ohishi, Y. (2020) New developments in high-pressure X-ray diffraction beamline for diamond anvil cell at SPring-8. *Matter and Radiation at Extremes* 5, 018403. https://doi.org/10.1063/1.5126038

Iizuka-Oku, R., Yagi, T., Gotou, H., Okuchi, T., Hattori, T., Sano-Furukawa, A. (2017) Hydrogenation of iron in the early stage of Earth's evolution. *Nature Communications* 8, 14096. https://doi.org/10.1038/ncomms14096

Ikuta, D., Ohtani, E., Sano-Furukawa, A., Shibazaki, Y., Terasaki, H., Yuan, L., Hattori, T. (2019) Interstitial hydrogen atoms in face-centered cubic iron in the Earth's core. *Scientific Reports* 9, 7108. https://doi.org/10.1038/s41598-019-43601-z

Jing, Z., Wang, Y., Kono, Y., Yu, T., Sakamaki, T., Park, C., Rivers, M.L., Sutton, S.R., Shen, G. (2014) Sound velocity of Fe–S liquids at high pressure: implications for the Moon's molten outer core. *Earth and Planetary Science Letters* 396, 78–87. https://doi.org/10.1016/j.epsl.2014.04.015

Katayama, Y., Saitoh, H., Yomogida, Y., Aoki, K. (2010) Structure of liquid iron hydrogen alloy under high pressure. *Journal of Physics: Conference Series* 215, 012080. https://doi.org/10.1088/1742-6596/215/1/012080

Kuwayama, Y., Morard, G., Nakajima, Y., Hirose, K., Baron, A.Q.R., Kawaguchi, S.I., Tsuchiya, T., Ishikawa, D., Hirao, N., Ohishi, Y. (2020) Equation of state of liquid iron under extreme conditions. *Physical Review Letters* 124, 165701. https://doi.org/10.1103/PhysRevLett.124.165701

Longhi, J. (2003) A new view of lunar ferroan anorthosites: post magma ocean petrogenesis. *Journal of Geophysical Research: Planets* 108, 5083. https://doi.org/10.1029/2002JE001941

Mita, S., Tagawa, S., Hirose, K., Ikuta, N. (2025) Fe–FeH eutectic melting curve and the estimates of Earth's core temperature and composition. *Journal of Geophysical Research: Solid Earth* 130, e2024JB029283. https://doi.org/10.1029/2024JB029283

Ohta, K., Ichimaru, K., Einaga, M., Kawaguchi, S., Shimizu, K., Matsuoka, T., Hirao, N., Ohishi, Y. (2015) Phase boundary of hot dense fluid hydrogen. *Scientific Reports* 5, 16560. https://doi.org/10.1038/srep16560

Pease, A., Liu, J., Lv, M., Piper, J., Kono, Y., Dorfman, S.M. (2025) Liquid structure of iron and iron–nitrogen–carbon alloys within the cores of small terrestrial bodies. *Journal of Geophysical Research: Planets* 130, e2024JE008599. https://doi.org/10.1029/2024JE008599

Rai, N., van Westrenen, W. (2014) Lunar core formation: new constraints from metal-silicate partitioning of siderophile elements. *Earth and Planetary Science Letters* 388, 343–352. https://doi.org/10.1016/j.epsl.2013.12.001

Seto, Y., Nishio-Hamane, D., Nagai, T., Sata, N. (2010) Development of a software suite on X-ray diffraction experiments. *The Review of High Pressure Science and Technology* 20, 269–276. https://doi.org/10.4131/jshpreview.20.269

Shibazaki, Y., Kono, Y. (2018) Effect of silicon, carbon, and sulfur on structure of liquid iron and implications for structure-property relations in liquid iron-light element alloys. *Journal of Geophysical Research: Solid Earth* 123, 4697–4706. https://doi.org/10.1029/2018JB015456

Stoutenburg, E.R., Caracas, R., Campbell, A.J. (2026) Immiscibility between hydrogen and molten iron in planetary cores. *Earth and Planetary Science Letters* 678, 119851. https://doi.org/10.1016/j.epsl.2026.119851

Tagawa, S., Sakamoto, N., Hirose, K., Yokoo, S., Hernlund, J., Ohishi, Y., Yurimoto, H. (2021) Experimental evidence for hydrogen incorporation into Earth's core. *Nature Communications* 12, 2588. https://doi.org/10.1038/s41467-021-22035-0

Tagawa, S., Helffrich, G., Hirose, K., Ohishi, Y. (2022) High-pressure melting curve of FeH: implications for eutectic melting between Fe and non-magnetic FeH. *Journal of Geophysical Research: Solid Earth* 127, e2022JB024365. https://doi.org/10.1029/2022JB024365

Tateno, S., Hirose, K., Sinmyo, R., Morard, G., Hirao, N., Ohishi, Y. (2018) Melting experiments on Fe–Si–S alloys to core pressures: Silicon in the core? *American Mineralogist* 103, 742–748. https://doi.org/10.2138/am-2018-6299

Tateno, S., Komabayashi, T., Hirose, K., Hirao, N., Ohishi, Y. (2019) Static compression of B2 KCl to 230 GPa and its *P-V-T* equation of state. *American Mineralogist* 104, 718–723. https://doi.org/10.2138/am-2019-6779

Tsujino, N., Nishihara, Y., Nakajima, Y., Takahashi, E., Funakoshi, K.-i., Higo, Y. (2013) Equation of state of γ-Fe: reference density for planetary cores. *Earth and Planetary Science Letters* 375, 244–253. https://doi.org/10.1016/j.epsl.2013.05.040

Tsutsumi, Y., Sakamoto, N., Hirose, K., Mita, S., Yokoo, S., Hsu, H., Yurimoto, H. (2025) Origin of Earth's hydrogen and carbon constrained by their core-mantle partitioning and bulk Earth abundance. *Nature Communications* 16, 10038. https://doi.org/10.1038/s41467-025-65729-5

Walker, D., Cranswick, L.M., Verma, P.K., Clark, S.M., Buhre, S. (2002) Thermal equations of state for B1 and B2 KCl. *American Mineralogist* 87, 805–812. https://doi.org/10.2138/am-2002-0701